Materials Science & Engineering A 592 (2014) 111–120

Contents lists available at ScienceDirect

Materials Science & Engineering A

journal homepage: www.elsevier.com/locate/msea

Compressive behavior of aluminum/copper hybrid foams under high strain rate loading

Yi Sun [a], Rigoberto Burgueño [a,*], Andy J. Vanderklok [b], Srinivasan Arjun Tekalur [b], Wei Wang [c], Ilsoon Lee [c]

[a] Department of Civil and Environmental Engineering, Michigan State University, 428 S. Shaw Lane, East Lansing, MI, USA
[b] Department of Mechanical Engineering, Michigan State University, 428 S. Shaw Lane, East Lansing, MI, USA
[c] Department of Chemical Engineering & Material Science, Michigan State University, 428 S. Shaw Lane, East Lansing, MI, USA

ARTICLE INFO

Article history:
Received 5 March 2013
Received in revised form
30 October 2013
Accepted 31 October 2013
Available online 12 November 2013

Keywords:
Hybrid open-cell foams
Electrodeposition
Nanocrystalline materials
High strain rate
Energy absorption
Finite element methods

ABSTRACT

The accessible interconnected structure of open-cell metal foams offers the opportunity to create hybrid foam materials through electrodeposited metal coatings, which has great potential for the fabrication of functionally-graded foam systems. Nanocopper coated aluminum (Al) foam was created by reinforcing conventional open-cell Al foams with electrodeposited nanocrystalline copper (Cu). The mechanical properties of such Al/Cu hybrid foam under high strain-rate compression were investigated using a split Hopkinson pressure bar and numerical methods were used to gain a further understanding on the micro-scale failure mechanisms. It was found that the stable compressive response of open-cell Al foam can be effectively enhanced by electrodeposited nanocopper coatings. However, such enhancement is limited by the relatively high brittleness of the Al/Cu hybrid foam due to the low ductility level of the electrodeposited nano-coating material. Nonetheless, this study also shows that the overall energy absorption performance of Al/Cu hybrid foams under high strain rate loading can be significantly improved by increasing the ductility level of the electrodeposited copper coating.

1. Introduction

The large amount of energy dissipated during the plastic deformation of metallic foams under compressive loading provides them with great energy absorption capacity and impact resistance. As a result, metallic foams can be used to protect personnel or important structural components in situations such as crashes or blast impact. The compressive behavior of cellular materials such as metallic foams is affected by the base material properties, the cell size, and the relative density [1–6]. Lately, increased attention has been paid to the development of strategically engineered functionally-graded metal foam systems with enhanced energy absorption capacity or the ability to tailor the propagation of stress waves through the foam [7–9]. While methods to fabricate functionally-graded foams by changing the pore size and density distribution in the foam have been reported [10,11], an alternative way with great potential is to create a hybrid foam by reinforcing the conventional open-cell foam with nano-scale through electrodeposition [12–14]. Boonyongmaneerat et al. [12], Bouwhuis et al. [13] and Jung et al. [14] investigated the quasi-static and high strain rate performance of open-cell aluminum (Al) foam reinforced with nanocrystalline nickel–tungsten (Ni–W) or nanocrystalline nickel (Ni) coating and found significantly enhanced modulus, strength and energy absorption capacity. Wang et al. [15] found similar enhancements under quasi-static loading for aluminum open-cell foams reinforced with nanocrystalline copper (Cu).

The work by Boonyongmaneerat et al. [12], Bouwhuis et al. [13], Jung et al. [14] and Wang et al. [15] demonstrates the effectiveness in manipulating the properties of open-cell Al foams using electrodeposited nano-crystalline metal coatings. However, it can be observed from their reported work that the hybrid foams had a distinctive behavior that differs considerably from that of conventional (uncoated) metal foams. The typical behavior of a metal foam (e.g., Al open-cell foam) can be described by three stages [1–6]: an elastic stage, followed by a collapse stage (or stress plateau stage) where a relatively constant stress level can be maintained up to a large strain level, and then the densification stage where the stress level rises rapidly due to the contact between cell walls (closed cell foam) or ligaments (open-cell foam). However, a large stress drop after the initial peak, especially for specimens with thicker coatings, was observed in the behavior of the Al/Ni–W and Al/Ni hybrid foams reported by Boonyongmaneerat et al. [12], Bouwhuis et al. [13] and Jung et al. [14] and the Al/Cu hybrid foams reported by Wang et al. [15], as shown in Fig. 1. No detailed discussion on this behavior was made in the noted

* Corresponding author. Tel.: +1 517 353 1743; fax: +1 517 432 1827.
E-mail address: burgueno@msu.edu (R. Burgueño).

0921-5093/$ - see front matter © 2013 Elsevier B.V. All rights reserved.
http://dx.doi.org/10.1016/j.msea.2013.10.104

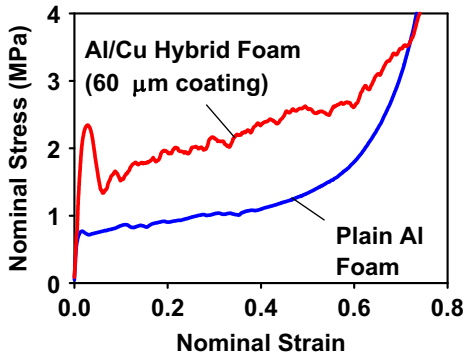

Fig. 1. Stress–strain curve of 40 pores per inch (PPI) plain Al foam and Al/Cu hybrid foam with 60 μm coating under compressive loading [15].

studies except for the observation noted by Bouwhuis et al. [13] of cracks and wrinkling of the Ni sleeve (coating) after the peak stress was reached. Energy absorption in metal foams is generally defined as the area under the stress–strain response up to the onset of densification. Thus, it is clear that the large stress drop greatly decreases the energy absorption capacity and efficiency of hybrid foams and the failure mechanism needs to be investigated in detail in order to get a better understanding of their performance and for possible improvement of their manufacturing process.

The Ni–W, Ni or Cu coatings in the hybrid foams in the studies previously mentioned were applied using direct current or pulsed electrodeposition and had a nanocrystalline structure. According to the Hall–Petch relationship [16,17] (see Eq. (1), where C is a constant and d is the mean grain size), the strength of a material increases with smaller grain size. However, the higher strength of electrodeposited nanocrystalline material is usually accompanied by a significantly reduced ductility capacity [18–21]. The increased brittleness may cause local coating failure in the hybrid foam material and lead to concentrated deformations in weakened critical sections at low strain levels. As most of the energy absorbed by metal foams is in the form of large plastic deformations, the consequences of a brittle coating in hybrid foams may overtake the enhancement gained from the additional strength and inhibit the improvement of energy absorption capacity.

$$\sigma_y = \sigma_0 + \frac{C}{\sqrt{d}} \tag{1}$$

It is hypothesized that the energy absorption capacity of aluminum open-cell foams under high strain rate loading can be effectively enhanced by electrodeposited metal coatings. However, the low ductility capacity of nanocrystalline coatings is detrimental to the performance of the fabricated hybrid foams, and thus the performance of such hybrid foams can be further enhanced by improving the ductility of the coating material.

In this study, Al/Cu hybrid foams were manufactured by electrodepositing copper on aluminum open-cell foams to investigate the compressive response and failure mechanism of the composite material under high strain rate loading. Copper was chosen as the coating material for ease in the electrodeposition procedure and relatively low expense. Compared to the current literature the present work provides an extended experimental evaluation on the dynamic behavior of hybrid foams with different coating thicknesses to provide guidance on the design of functionally graded foam material systems under high-rate compressive strains. Further, the failure mechanism in hybrid foams with different coating thickness was studied at the micro-scale level using finite element (FE) models of a single foam ligament. In order to study the influence of the ductility capacity of the nano-copper coating, an annealing process was performed on part of the specimens after electrodeposition and the behavior was compared with that of specimens without annealing.

2. Material and methods

2.1. Materials

Open-cell aluminum foams fabricated with Al 6101-T6 alloy (Duocel aluminum foam, ERG Materials and Aerospace Corp, Oakland, CA, US) with a pore size of 40 PPI (pores per inch) and a relative density of about 6% were used as base materials for this investigation. Foam specimens with desired dimensions were cut from foam blocks (25.4 mm by 25.4 mm by 50.8 mm) using an electrical discharge machining and coated with copper using the electrodeposition procedure described in Section 2.2.

2.2. Electrodeposition

The Al/Cu hybrid foams were manufactured by applying a nanocrystalline copper coating on an aluminum open-cell foam using electrodeposition (see Fig. 2) following the procedure custom-designed by Wang et al. [15]. It is acknowledged that the processing set-up used in this study is similar to the one developed by Jung et al. [14,22] in the manufacturing of Al/Ni hybrid foams. Briefly, pre-treatment according to ASTM Standard B 253 was applied to the foam specimens prior to electrodeposition to yield a better coating result. A commercial electrolyte (Uyemura International Co., Ontario, CA, US), which mainly contained copper pyrophosphate as the copper source was used at 65 °C and a pH of 7.5. A titanium basket with copper strips tied on the sides was used as the anode and the foam specimen was placed in the center of the basket without any contact with it. A stirring bar was applied throughout the entire deposition process at 180 rpm to minimize the gradient of electrolyte concentration. The electrodeposition was carried out at a constant current density of about 13 mA/cm^2.

The nominal copper coating thicknesses of Al/Cu hybrid foam samples was calculated based on the gained weight. Assuming the copper coating is uniformly applied on the foam ligaments with circular cross sections of radius r, the weight of copper coating is

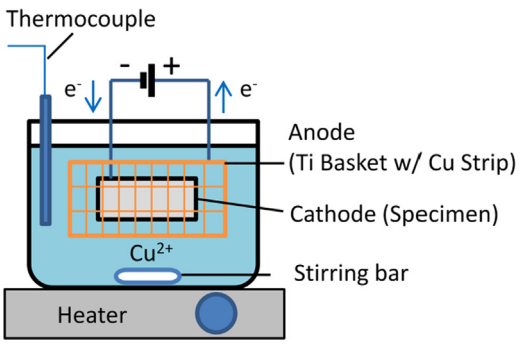

Fig. 2. Schematic of electrodeposition setup.

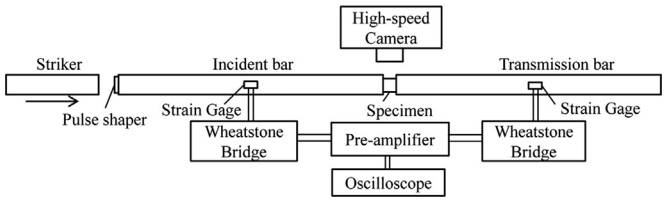

Fig. 3. Schematic of split Hopkinson pressure bar (SHPB) setup.

proportional to the cross section area of the coating layer as shown in Eq. (2); where W is the copper weight density (g/cm^3), C is a constant and t_c is the coating thickness (μm). The radius r was defined to be 97 μm based on measurements of ligaments on 40 PPI foams by Wang et al. [15]. The constant in Eq. (2) was determined by fitting the equation with the measurements reported by Wang et al. [15] in which coated foam struts of representative samples were imaged with a scanning electron microscopy and measured coating thickness was averaged based on at least 30 measurements at different locations for each sample. The nominal thicknesses of the copper coatings considered in this study were 30, 60, and 120 μm.

$$W = C((r+t_c)^2 - r^2) = C(t_c^2 + 2rt_c),\ C = 2.76 \times 10^{-5} \quad (2)$$

2.3. High strain rate experiments

Compressive performance of the Al/Cu hybrid foams under high strain rate loading was investigated using a split Hopkinson pressure bar (SHPB). Fig. 3 shows a schematic of the SHPB set up, which consists of an incident bar, a transmission bar, and a striker. The incident bar and the striker were two solid aluminum bars with a diameter of 19 mm and lengths of 1829 mm and 508 mm, respectively. Due to the low impedance of the foam material studied, a hollow aluminum bar (I.D.=15 mm, O.D.=19 mm) with a length of 1829 mm was used as the transmission bar. A 1 mm thick copper plate was used as the pulse shaper. Strain gages were placed at the half length point of both the incident and transmission bars to measure the incident strain ε_i (t), the transmitted strain ε_t (t) and the reflected strain ε_r (t). To reduce noise in the measured signal, four strain gages were placed on the transmission bar and connected to a full bridge configuration while a half bridge configuration was used for the strain gage on the incident bar. In order to achieve equilibrium during the SHPB experiments the specimen length (L_S) needs to be small, especially for materials with low impedance [23]. However, when evaluating foams it is necessary that the test sample contains several cells in the loading direction. As a result, the SHPB specimens used in this study (see Fig. 4a) had a diameter of 15.9 mm and a length of 5 mm (about eight times the pore size), which was the same length used in the study by Jung et al. [14].

Fig. 5 shows an oscilloscope record obtained during one of the SHPB experiments. The flat plateau of the incidence and reflected pulse indicates a constant strain rate of about 180 μs for the noted setup. The stress, strain and strain rate of the specimen were reconstructed from the strain-time records using Eqs. (3)–(5) [24]:

$$\sigma_s(t) = E_t \frac{A_t}{A_s} \varepsilon_t(t) \quad (3)$$

$$\varepsilon_s(t) = \frac{2C_0}{L_s} \int_0^t [\varepsilon_i(t) - \varepsilon_r(t) - \varepsilon_t(t)]dt \quad (4)$$

$$\dot{\varepsilon}_s(t) = \frac{2C_0}{L_s} [\varepsilon_i(t) + \varepsilon_r(t) - \varepsilon_t(t)] \quad (5)$$

where C_0 is the wave speed within the bar; A_t and A_s are the cross-sectional areas of the specimen and the transmission bar, respectively; and E_t is Young's modulus of the transmission bar. Four different types of specimens were considered: uncoated, and Cu coated with 30 μm, 60 μm, and 120 μm nominal coating thicknesses; and three experiments were conducted for each specimen type. Two different strain rates were obtained in the SHPB experiments conducted in this study, namely, 2.8×10^3 s^{-1} and 4.9×10^3 s^{-1}.

2.4. Quasi-static experiments

To provide a reference for the high strain rate experiments, quasi-static compressive experiments were also performed with a universal testing frame. It is important to maintain the same specimen length in the loading direction in both the high strain

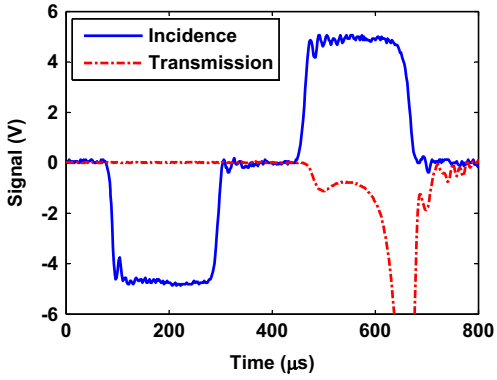

Fig. 5. Typical oscilloscope records from SHPB experiments. The plateaus of the incident pulse and reflected pulse indicated a constant strain rate for about 180 μs.

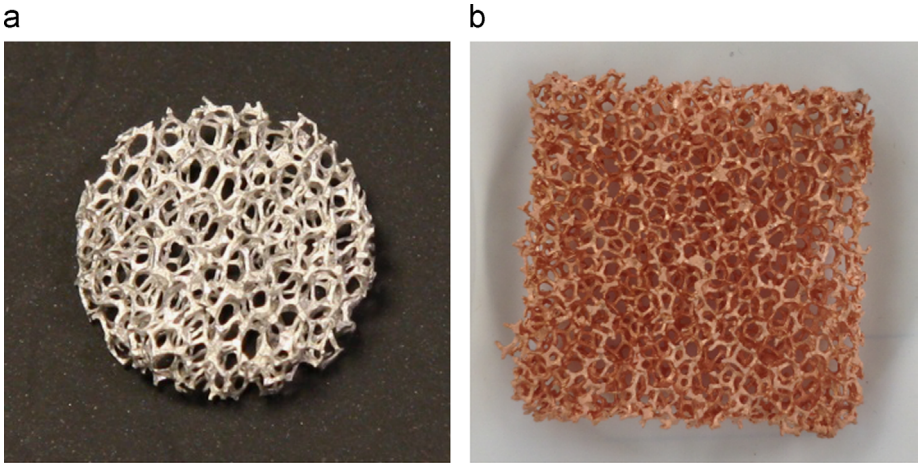

Fig. 4. Cross section pictures of (a) uncoated circular-shaped (5 mm thick with a diameter of 15.9 mm) specimen for dynamic experiments and (b) Cu-coated square-shaped specimen (25.4 mm × 25.4 mm × 5 mm) for quasi-static experiments. The loading directions for both dynamic and quasi-static experiments were through the thicknesses. All specimens were fabricated based on 40 PPI open-cell Al 6101-T6 foams with a relative density of about 6% (Duocel aluminum foam, ERG Materials and Aerospace Corp, Oakland, CA, US).

rate and quasi-static experiments as the non-uniform collapse of cells in foam specimens of larger size may lead to a different overall behavior [6]. Thus, the specimens used for the quasi-static experiments (Fig. 4b) also had a thickness of 5 mm and a cross-section of 25.4 mm by 25.4 mm. The experiments were conducted in a displacement control mode at a strain rate of $3.3 \times 10^{-3}\ s^{-1}$. Three experiments were conducted for each specimen type.

2.5. Ductility enhancement

The low ductility capacity of the electrodeposited metal coating is considered to be unfavorable for the overall energy absorption performance of hybrid foams as most of the energy absorbed is due to large plastic deformation of the cell struts. Thus, it is necessary to investigate the effect of ductility capacity of the coating material on the performance of the hybrid foam. In this study, an annealing process was added to some of the specimens after the electrodeposition process. Annealing is a well-established heat treatment process for metals to release internal stresses and enhance ductility through recrystallization and grain growth, which also usually results in a lower strength due to the change of crystal structure [25–27]. Annealing was conducted at a temperature of 400 °C in a vacuum furnace (3×10^{-5} Torr) for 1 h. The noted temperature was chosen since it is about half of the melting temperature of copper (1084 °C) at which the recrystallization can occur [25] and at the same time it is not too close to the melting temperature of aluminum (660 °C). The temperature was increased at a rate of about 10 °C/min and the furnace was cooled down slowly after the annealing process. It needs to be noted that the annealing process was used to investigate the effect of enhanced coating ductility in hybrid foams. However, it was not within the scope of this study to perform a thorough investigation on the effect of different annealing process parameters on the mechanical properties of nano-copper coatings.

X-ray diffraction (XRD) was used to evaluate the effect of annealing on the crystallite size of the copper coating in the Cu/Al hybrid foam. Fig. 6 shows the first two peaks of the XRD diagram obtained for two Cu/Al hybrid foam specimens, one of which was annealed after electrodeposition while the other one was not. The peak positions of the observed pattern are summarized in Table 1 together with the peak positions for copper reported in the literature [28]. It can be seen that the peak positions in the pattern of the Al/Cu foams agree well with those for copper since the aluminum was completely covered by the copper coating. The crystallite size of nano-copper coating was determined using the averaged estimation of the first three peaks and the Scherrer formula (Eq. (6)) [29], where τ is the mean

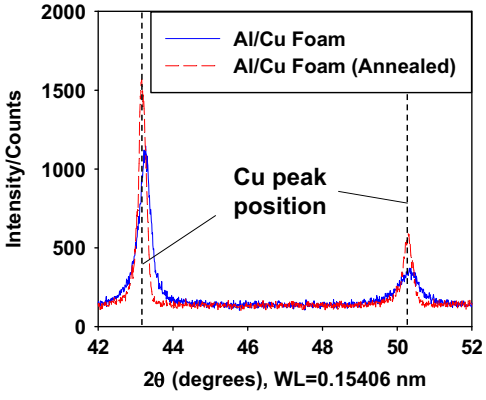

Fig. 6. First two peaks of XRD patterns of copper (Cu) coated aluminum (Al) foam specimens with and without annealing. The peaks positions for Cu were obtained from published literature [27].

Table 1
Summary of results from XRD measurements on Al/Cu hybrid foam specimens.

Material	1st Peak position	2nd Peak position	3rd Peak position	Estimated average Cu crystallite size (nm)
Al/Cu hybrid foam	43.23°	50.32°	73.99°	26
Al/Cu hybrid foam (Annealed)	43.15°	50.26°	73.97°	51
Copper [27]	43.30°	50.43°	74.13°	–

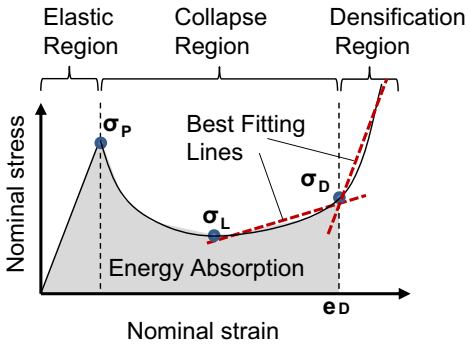

Fig. 7. Schematic of typical compressive behavior of Al/Cu hybrid foams with peak stress (σ_P), lowest stress in collapse region (σ_L), densification stress (σ_D) and densification strain (ε_D).

crystallite size, K is shape factor, λ is the X-ray wavelength (0.15406 nm), β is the line broadening at half the maximum intensity (FWHM), and θ is the Bragg angle. It can be seen in Table 1 that the annealed specimen had a significantly increased crystallite size, which indicates the occurrence of grain growth from annealing.

$$\tau = \frac{K\lambda}{\beta \cos \theta} \tag{6}$$

3. Results and discussion

3.1. Compressive behavior of hybrid foams

Fig. 7 shows a typical compressive stress strain curve for the Al/Cu hybrid foams reported in this study. Nominal stress (load divided by original cross-sectional area) and nominal strain (deformation divided by original length) are used throughout the results presented here. Similar to the behavior of a conventional single-material metal foam, the response features an elastic region, a collapse region and a densification region. However, it was observed that the stress level in the collapse region dropped significantly after the initial peak stress σ_P for the hybrid foams, while such difference is usually small in conventional single-material metal foams [1,6]. Ideally the stress level should remain constant at a nominal level close to the initial peak stress throughout the collapse region to maximize the energy absorbed during plastic deformations under a constant stress level. Thus, the significant drop after the initial peak stress is considered an unfavorable behavior feature and needs to be considered when evaluating the energy absorption performance of hybrid foams.

In this study, the densification strain ε_D was defined as the strain level at the intersection of the best fitting lines (using a least square fit) of the ascending part in the collapse region and the densification region, respectively, as shown in Fig. 7. The energy absorption capacity was defined as the area under the stress–strain

Table 2
Summary of results from all experiments. "S" refers to quasi-static experiments (strain rate of 3.3×10^{-3} s^{-1}) while "D" refers to dynamic experiments. The numbers in the ID name after "C" represent the nominal thickness of nano-copper coating in μm and the other number indicates the strain rate ("28" and "49" refer to strain rates of 2.8×10^3 s^{-1} and 4.9×10^3 s^{-1}, respectively). Sample ID name with "A" refers to annealed samples.

Sample ID	σ_P (MPa)	σ_L (MPa)	$\Delta\sigma$ (%)	ε_D (mm/mm)	Energy absorption (N mm)	Ideal energy (N mm)	Efficiency (%)
S.C0	0.64	0.63	2	0.68	0.70	2.11	33
S.C30	2.66	1.35	49	0.68	1.28	2.65	48
S.C60	4.21	1.83	57	0.65	1.71	3.79	45
S.C120	10.59	4.32	59	0.62	3.68	6.57	56
D.C0.28	0.67	0.54	19	–	–	–	–
D.C30.28	1.96	0.74	62	–	–	–	–
D.C60.28	4.00	1.14	71	–	–	–	–
D.C120.28	10.82	1.68	85	–	–	–	–
D.C0.49	0.73	0.52	29	0.68	0.69	2.52	27
D.C0.49	2.97	0.73	75	0.65	1.11	2.80	40
D.C60.49	4.39	1.02	77	0.61	1.31	2.68	49
D.C120.49	12.68	1.91	85	0.61	2.79	7.73	36
D.C30.49.A	2.10	1.16	45	0.59	1.22	2.56	48
D.C60.49.A	4.43	2.29	48	0.55	1.93	3.70	52
D.C120.49.A	9.10	5.92	35	0.52	3.94	6.10	65

curve up to the densification strain. In addition, energy absorption efficiency was defined as the ratio of the absorbed energy to an ideal energy absorption level, which was defined as the product of the densification strain ε_D and the initial peak stress σ_P, or the stress at densification strain σ_D, whichever is larger (see Eq. (7)). While a detailed discussion on the compressive behavior will be presented and discussed in the following sections, the quantitative parameters of all experiments are summarized in Table 2, where σ_L is the lowest stress level in the collapse region and $\Delta\sigma$ is the ratio of the stress drop to the initial peak stress calculated using Eq. (8). The letters "S" and "D" in the sample identification (ID) names represent quasi-static (with strain rate of 3.3×10^{-3} s^{-1}) and dynamic experiments, respectively. The number after letter "C" represents the nominal thickness of the nano-copper coating in μm and the last number indicates the strain rate ("28" and "49" refer to strain rates of 2.8×10^3 s^{-1} and 4.9×10^3 s^{-1}, respectively). Sample ID names with an "A" refer to annealed samples. All data is based on the average of three repeated experiments for each specimen type. It needs to be noted that at the strain rate of 2.8×10^3 s^{-1} the densification region in the dynamic response of Al/Cu hybrid foams could not be fully captured with the current setup and thus the densification strain ε_D and the energy absorption capacity could not be determined at such strain rate.

$$Efficiency = \frac{Energy\ absorption}{\max(\sigma_P, \sigma_D)\varepsilon_D} \tag{7}$$

$$\Delta\sigma = \frac{\sigma_P - \sigma_L}{\sigma_P} \times 100\% \tag{8}$$

3.2. Effect of electrodeposited copper coating

The stress–strain curves obtained from quasi-static and high-strain rate compression experiments are shown in Fig. 8. The naming convention for the different experiments can be found in Section 3.1. The behavior for each specimen type presented in this paper is the average of three separate experiments. Specimen size was dictated by the high-rate experiment requirements. As the foam response is affected by sample size, the behavior reported here differs from that obtained by Wang et al. [15] with larger specimens. Yet, the objectives of this work are not thought to be compromised by this fact since the results are used for mutual comparison. It can be seen from Fig. 8 that the performance of the aluminum foam under both quasi-static and high strain rate compressive loading was effectively enhanced by the electrodeposited copper coating. In general, the initial peak stress and the plateau stress of the coated foam specimen increased with the coating thickness. This is expected as the moment of inertia of a reinforced ligament section is larger and thus its load bearing capacity (controlled by flexural yielding) is increased. Meanwhile, a slight decrease of the densification strain for specimens with thicker coating was observed in both quasi-static and dynamic experiments, which is attributed to the fact that the densification of a foam is basically a volumetric phenomenon and that specimens with thicker coating have more material.

As mentioned in Section 3.1, a significant stress drop in the compressive stress–strain curve was observed in all experiments on coated samples and such drop was more significant for specimens with thicker coatings. Similar behavior was reported in previous studies on open-cell Al foam with nanocrystalline Ni coatings by Bouwhuis et al. [13] and Jung et al. [14] and the study on Al/Cu hybrid foams by Wang et al. [15]. Considering the previously noted definition of energy absorption capacity, a high peak stress followed by a large drop can significantly reduce the foam's energy absorption efficiency. As demonstrated in the annealing effect evaluation (Section 3.3) and numerical studies (Section 3.4) presented later, the observed stress drop is mainly attributed to the rupture of the electrodeposited coating material, as electrodeposition usually leads to a material with low ductility [19]. The larger stress drop for specimens with thicker coatings is due to the increased capacity loss of the ligament, and the foam, upon brittle failure of the thicker section reinforcement. It was also observed that the stress drop was more significant under high strain rate loading (see Fig. 8). This may be attributed to the fact that the shattering of foam ligaments and the spalling of coating material was more severe under high strain rate loading. Such phenomenon also led to a slightly higher densification strain in Al/Cu hybrid foams under high strain rate loading conditions, especially with thicker coatings. It can be seen from Table 2 that the lower plateau stress from high strain rate experiments lead to a relatively lower energy absorption capacity and efficiency compared to the quasi-static experiments.

Fig. 9 compares the performance of foam specimens with different coating thickness under different loading rates. No significant difference on the initial peak stress (see Fig. 9a) with respect to loading rates was observed for plain Al foams and Al/Cu hybrid foams with nominal copper coating thicknesses less than 120 μm. However, the hybrid foams with 120 μm nominal coating thickness showed slightly higher initial peak stress at a strain rate of 4.9×10^3 s^{-1} compared to that at lower strain rates. Fig. 9b shows that the lowest stress level in the collapse region of the coated foams was lower in the dynamic experiments, which can again be explained by the more severe specimen shattering and material spalling under high-rate loading. No significant difference

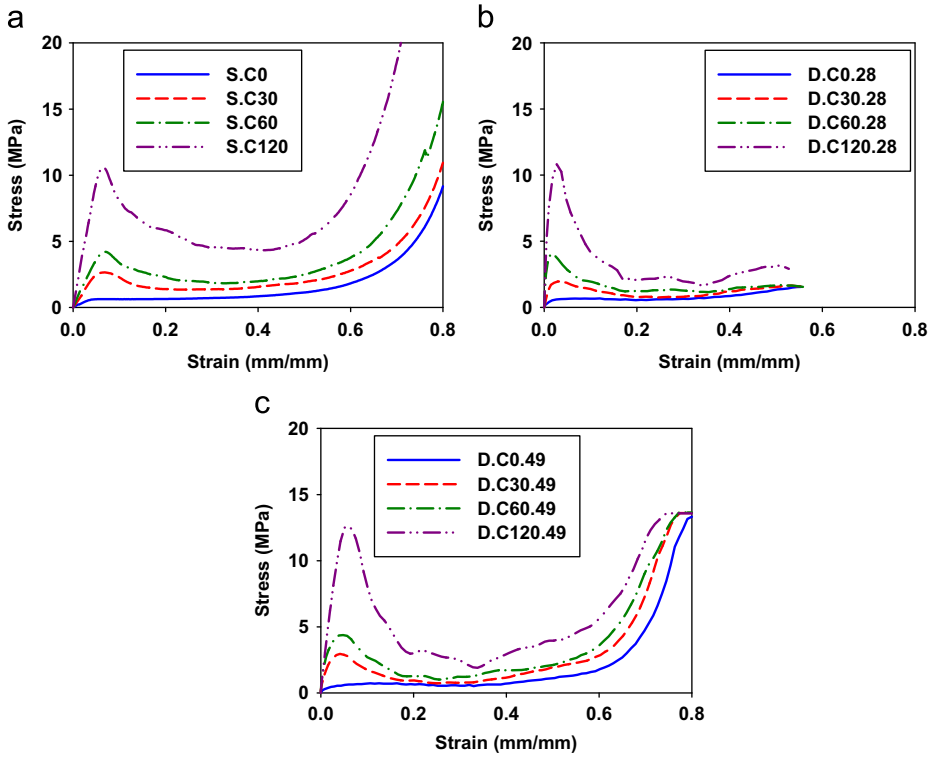

Fig. 8. Compressive behavior of Al/Cu hybrid foams with different coating thickness under (a) quasi-static loading with a strain rate of $3.3 \times 10^{-3}\ s^{-1}$ and high-strain rate loading with a strain rate of (b) $2.8 \times 10^{3}\ s^{-1}$ and (c) $4.9 \times 10^{3}\ s^{-1}$. "S" refers to quasi-static experiments while "D" refers to dynamic experiments and the values after "C" in the legends indicate the nominal copper coating thicknesses in μm. "28" and "49" indicate a strain rate of $2.8 \times 10^{3}\ s^{-1}$ and $4.9 \times 10^{3}\ s^{-1}$, respectively.

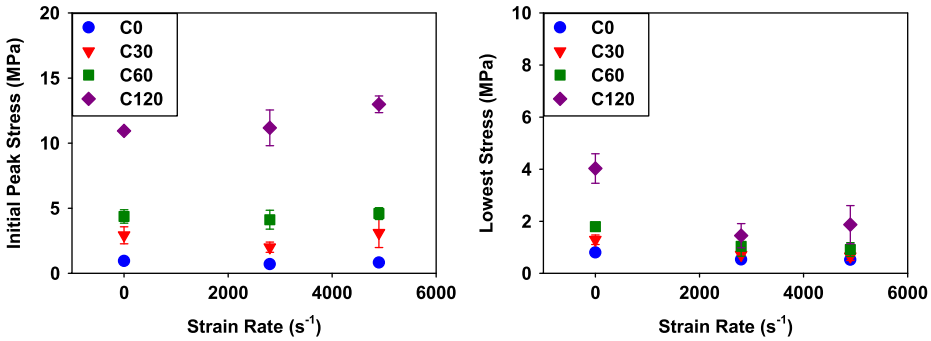

Fig. 9. Initial peak stress and lowest stress level in the compressive behavior of Al/Cu hybrid foams under different strain rates. The values after "C" in the legends indicate the nominal copper coating thicknesses in μm. The error bars in the plots show the standard deviation of the averaged results.

in the lowest stress values was observed under strain rates of $2.8 \times 10^{3}\ s^{-1}$ and $4.9 \times 10^{3}\ s^{-1}$.

3.3. *Effect of annealing*

The compressive behavior of annealed and un-annealed Cu/Al hybrid foams under high strain rate loading ($4.9 \times 10^{3}\ s^{-1}$) is shown in Fig. 10. For reference purposes, the result of a plain aluminum foam specimen is included in all plots. First, it can be seen from the plots in Fig. 10 that the annealed specimens generally show a similar or lower peak stress compared to the un-annealed specimens. This is because the recrystallization and grain growth that occurs during the annealing process changes the crystal structure and leads to a lower yield strength [25–27]. Secondly, it can be seen that the stress plateau after the peak stress was higher for the annealed foam specimens. As a result, the annealing process reduced the difference between the initial peak stress and the stress level in the collapse region, which is beneficial for energy absorption efficiency. It can also be seen that the effect of annealing was more significant for foam specimens with thicker coatings as the improvement in ductility is mainly on the copper coating. Thirdly, it can be observed that the densification onset starts earlier in the annealed specimens, which can also be seen in Table 2. The lower densification strain may reduce the improvement in energy absorption capacity. However, it was observed that the annealed specimens stayed intact during the experiments even at high strain loading, while dramatic shattering occurred in the un-annealed specimens (especially the ones with the thickest coating, see Fig. 11). Thus, considering the amount of material broken away from the loaded domain, the densification strain obtained in the plots for the un-annealed specimens may be overestimated. In addition, it is considered that the relatively ductile nature of the annealed hybrid foams under compression is favorable as it may avoid local concentrated damage and thus further improve the energy absorption efficiency of the material.

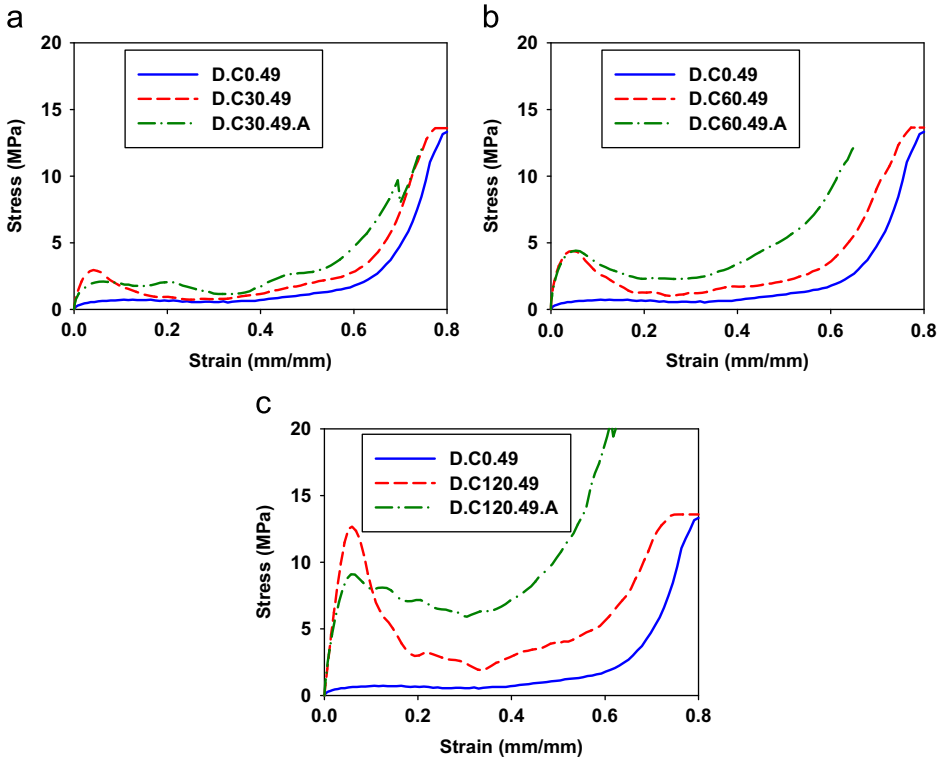

Fig. 10. Comparison of compressive behavior under high strain rate loading ($4.9 \times 10^3\ s^{-1}$) of annealed specimen and un-annealed specimen with nominal copper coating thicknesses of (a) 30 μm, (b) 60 μm, and (c) 120 μm. "D" refers to dynamic experiments; the values after "C" in the legends indicate the nominal copper coating thicknesses in μm; "49" indicates a strain rate of $4.9 \times 10^3\ s^{-1}$; and "A" refers to annealed samples.

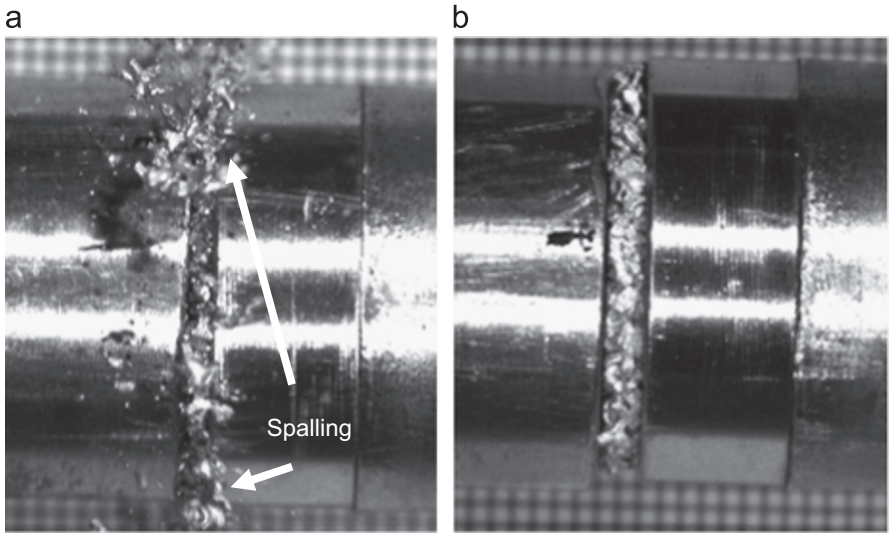

Fig. 11. Images of (a) un-annealed and (b) annealed Al/Cu hybrid foam specimens with 120 μm nominal copper coating thickness during high-rate compressive loading. Significant shattering and spalling was observed for the un-annealed specimen while the annealed specimen basically stayed intact.

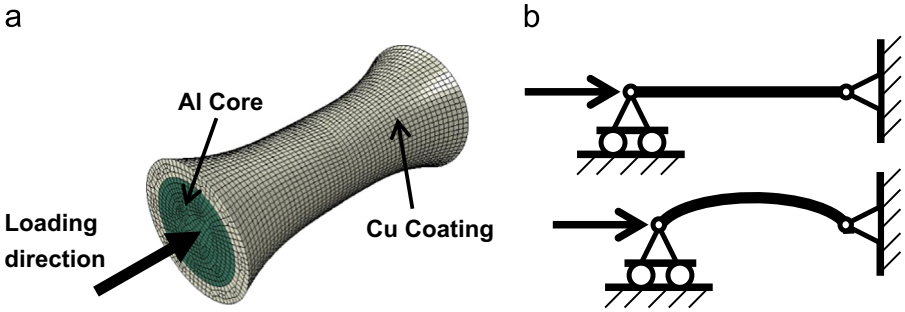

Fig. 12. Finite element model of (a) single ligament in open-cell foam structure and (b) illustration of pin-and-roller boundary conditions. Initial imperfection was defined along the ligament length to bring about the inelastic buckling mechanism.

3.4. Numerical investigation on the effect of coating ductility

It has been shown that annealing can be used to improve the performance of Al/Cu hybrid foams and that such enhancement can be attributed to the increased ductility in copper coating. However, the effect of coating ductility on the behavior and failure mechanism of Al/Cu hybrid foams at the micro level is not yet fully understood. Thus a numerical study was conducted on simplified models of a single ligament from a 40 PPI Al-6101-T6 foam (see Fig. 12a) using the commercial finite element software ABAQUS [30]. Both the aluminum core and the copper coating were discretized using C3D8R (eight-node linear bricks with reduced integration and hourglass control) solid elements. A circular shape cross-section was used for the numerical model and the cross-section was defined to be non-uniform along the length of the ligament based on the equation proposed by Jang and Kyriakides [6], in which the cross-sectional area at different locations can be calculated based on the distance from the mid-span and the cross-sectional area at the mid-span of the ligament. The diameter of the cross-section at mid-span of the base aluminum ligament was defined to be 193 μm, which was based on the measurements by Wang et al. [15] and the length of the ligament was taken as 1.04 mm, which is the average ligament length for a 40 PPI Al-6101-T6 foam as measured by Jang and Kyriakides [6]. The copper coating was defined by adding a sleeve with corresponding thickness around the aluminum core and a perfect bond was prescribed between the coating and core model parts. Two thicknesses were considered in the numerical study, namely, 30 μm and 60 μm. Pin and roller boundary conditions (see Fig. 12b) were defined for the numerical model, where both ends of the model were allowed to rotate while only one end could move along the axis of the ligament. The loading was defined by applying a displacement on the free end in the longitudinal direction. In order to invoke the inelastic buckling behavior, an initial imperfection was seeded for the ligament geometry based on the first buckling mode shape, which was obtained from a separate eigenvalue buckling analysis. It is understood that the ligaments in a real loaded foam specimen have more complicated boundary conditions and loading demands. However, the simplified numerical models in this study were used to gain a better understanding of the effect of coating ductility on the failure mechanisms and performance of Al/Cu hybrid foams rather than to accurately simulate the real high-rate micro-scale behavior. The simplified models presented here are considered sufficient for the purpose of this study since the major mechanism involved in the global, or macro-level, deformation of a metal foam is the inelastic buckling response of ligaments [1].

The material models defined for the aluminum core and copper coating were based on the results from micro-scale tensile experiments on single Al foam ligaments conducted by Zhou et al. [31] and on the tensile experiments on thin electrodeposited copper films by Zhang et al. [19], where it has been shown that the behavior of both aluminum and copper at these lower length scales are quite different from their bulk, or macro-scale, counterparts. Tensile damage properties [30] were defined for both aluminum and copper in the FE models to capture the onset of damage and allow elements to degrade and eventually fail once the defined fracture strain was reached. A summary of key parameters of the material definition used in this study is given in Table 3, where E is Young's modulus, σ_y is the yield strength and σ_u is the ultimate strength. An explicit dynamic analysis, which uses an explicit central-difference time integration rule [30], was used to perform the numerical simulations.

Fig. 13 shows the Mises stress at a center longitudinal section cut of the ligament models with different copper coating thicknesses (t) at different deformation stages, where D is the longitudinal displacement of the moving end and L is the length of the ligament. Elements with excessive deformation were removed from the view. It can be seen that the majority of the deformation happens in the middle region, which is the location of the maximum bending moment. It can also be seen that no fracture was observed in the uncoated case (first row) even at large deformations. However, fracture occurs in the coated models in the tensile side of the copper coating at the middle section even at small deformations, and this was followed by partial fracture of the aluminum core. This can be explained by recognizing that all of the deformation concentrates at the weakened middle section once rupture of the copper coating happens, as the rest of the strut is still reinforced. Fracture on the strut core is more severe as the copper coating gets thicker because the tensile stress on the strut core is higher to maintain a sectional equilibrium with more copper in compression. Fig. 14 shows plots of the overall axial force versus axial displacement for the struts and it can be seen that even though the peak load carrying capacity is significantly enhanced by the copper coating, the strut rapidly looses strength and degrades essentially to the same level as the uncoated strut at large deformations. The rapid strength loss of the strut is due to the noted failure mechanism at a critical section. This explains the increased stress drop and relatively more brittle behavior observed in the experiments of un-annealed specimens with thicker coatings.

Table 3
Material definition for aluminum and copper in finite element models.

Material	E (GPa)	σ_y (MPa)	σ_u (MPa)	Fracture strain in tension (mm/mm)
Aluminum	70	193	397	0.5
Copper	102	100	235	0.08

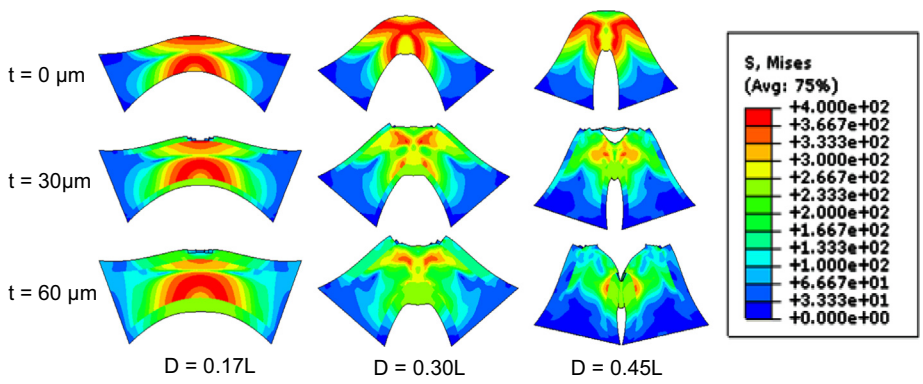

Fig. 13. Mises stress (MPa) contour of single ligament models with different coating thicknesses (t) at different free-end displacement (D) with respect to the length of the ligaments (L).

3.5. Discussion

Fig. 15 shows the comparison of energy absorption, stress drop ratio and energy absorption efficiency of Al/Cu hybrid foams with different coating thicknesses. The discussion herein is based on the experimental results from the two extreme strain rates in this study, namely, $3.3 \times 10^{-3}\ s^{-1}$ (quasi-static) and $4.9 \times 10^{3}\ s^{-1}$. It can be seen that the energy absorption capacity of the Al/Cu hybrid foams increases with coating thickness (see Fig. 15a). The energy absorption capacity of the Al/Cu hybrid foams from high strain rate experiments are lower than those from quasi-static experiments due to the specimen shattering and the material breaking away as mentioned earlier. Even though the initial peak stress was lower for the annealed specimens, the energy absorption capacity was significantly higher compared to the specimens without an annealing process.

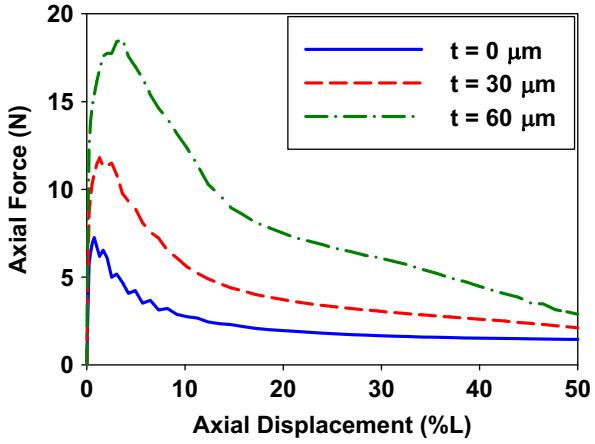

Fig. 14. Force–displacement plot of axial compressive response for single ligament models with different coating thicknesses (t). The axial displacement is shown as a percentage of the ligament length (L).

This indicates that ductility is as important as strength for the coating of hybrid metal foams. Compared to plain aluminum foams, specimens with a nominal coating thickness of 120 μm had an energy absorption capacity approximately four times larger under high strain rate loading and more than five times larger under quasi-static loading. The larger stress drop after the initial peak stress for un-annealed specimens with thicker coatings can be seen in Fig. 15b. Such stress drop significantly limits or even reduces the energy absorption efficiency as shown in Fig. 15c. However, by applying an annealing process the stress drop ratio was significantly reduced, especially for thicker coatings, which lead to a relatively uniform stress level in the collapse region. The enhanced ductility of the copper coating leads to a proportional increase in energy absorption efficiency with coating thickness as shown in Fig. 15c.

It has thus been shown that Al/Cu hybrid foams manufactured through electrodeposition have a better energy absorption performance that can be effectively modified by controlling the coating thicknesses and processing. Such controllable enhancement indicates the potential to fabricate functionally graded foams through a designed electrodeposition procedure that provides non-uniform reinforcing coatings.

4. Conclusions

The high strain rate compressive behavior of Al/Cu hybrid foams manufactured by electrodepositing nanocrystalline copper onto open-cell aluminum foam was investigated using experimental and numerical methods. The effect of ductility enhancement of the coating material on the performance of such hybrid foams was evaluated by introducing an annealing process. It was found that:

(1) The energy absorption capacity of aluminum open-cell foams under high strain rate loading can be effectively enhanced by electrodeposited copper coatings and that such enhancement increases with coating thickness.

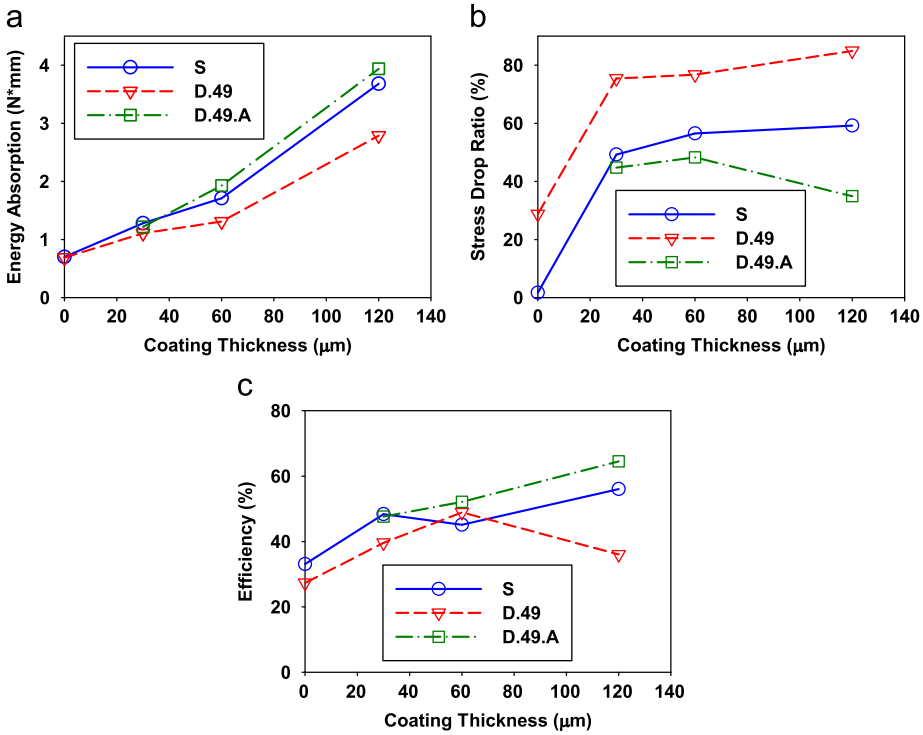

Fig. 15. Comparison of (a) energy absorption capacity, (b) stress drop ratio, and (c) energy absorption efficiency for quasi-static and high strain rate experiments. "S" refers to quasi-static experiments while "D" refers to dynamic experiments; "49" indicates a strain rate $4.9 \times 10^{3}\ s^{-1}$; and "A" refers to annealed samples.

(2) The compressive behavior of Al/Cu hybrid foams with a thick coating (120 μm) had a slightly increased initial peak stress at higher strain rates, while no significant difference in the initial peak stress was observed for hybrid foams with thinner coatings. However, in all cases the stress level in the collapse region was relatively low under high strain rate loading due to specimen shattering and the material breaking away, which lead to a lower energy absorption capacity compared to that under quasi-static loading.
(3) A large obvious drop in the stress level following the initial peak stress was observed in the compressive response of Al/Cu hybrid foams. Numerical analyses showed that this can be attributed to the rupture of the coating material and the concentration of deformations at weakened critical sections due to the low ductility of the electrodeposited nano-coating. Such phenomenon is more significant in foams with thicker coating and is unfavorable for the energy absorption performance of hybrid metal foams as it limits or even reduces their energy absorption efficiency.
(4) The ductility capacity of electrodeposited copper coatings has a great influence on the overall energy absorption efficiency of Al/Cu hybrid foams. Coatings with better ductility (e.g., obtained by adding an annealing process) lead to significant improvements in energy absorption capacity and efficiency, and a more favorable inelastic deformation mechanism. It is believed that such improvement can also be applied to other hybrid foams manufactured using a similar procedure. The more ductile failure mechanism due to the reduction in coating brittleness may be even more beneficial for hybrid foams with larger specimen size since brittle failure mechanisms may cause localized damage and thus reduce their energy absorption efficiency.

Acknowledgments

This research described in this paper was carried out under funding from the US National Science Foundation under Grant no. CMMI 0928835. The authors thank Prof. David Grummon (MSU) for providing access to the vacuum furnace used for the annealing of samples.

References

[1] L.J. Gibson, M.F. Ashby, Cellular Solids: Structure and Properties, second edition, Cambridge University Press, Cambridge, UK, 1999.
[2] L. Gong, S. Kyriakides, Int. J. Solids Struct. 42 (2005) 1381–1399.
[3] L. Gong, S. Kyriakides, W.Y. Jang, Int. J. Solids Struct. 42 (2005) 1355–1379.
[4] H. Yu, Z. Guo, B. Li, G. Yao, H. Luo, Y. Liu, Mater. Sci. Eng. A 454–455 (2007) 542–546.
[5] W.Y. Jang, A.M. Kraynik, S. Kyriakides, Int. J. Solids Struct. 45 (2008) 1845–1875.
[6] W.Y. Jang, S. Kyriakides, Int. J. Solids Struct. 46 (2009) 617–634.
[7] L. Cui, S. Kiernan, M.D. Gilchrist, Mater. Sci. Eng. A 507 (2009) 215–225.
[8] A.H. Brothers, D.C. Dunand, Mater. Sci. Eng. A 489 (2008) 439–443.
[9] S. Kieman, L. Cui, M.D. Gilchrist, Int. J. Non Linear Mech. 44 (2009) 456–468.
[10] A.H. Brothers, D.C. Dunand, Adv. Eng. Mater. 8 (2006) 805–809.
[11] Y. Hangai, K. Takahashi, T. Utsunomiya, S. Kitahara, O. Kuwazuru, N. Yoshikawa, Mater. Sci. Eng. A 534 (2012) 716–719.
[12] Y. Boonyongmaneerat, C.A. Schuh, D.C. Dunand, Scr. Mater. 59 (2008) 336–339.
[13] B.A. Bouwhuis, J.L. McCrea, G. Palumbo, G.D. Hibbard, Acta Mater. 57 (2009) 4046–4053.
[14] A. Jung, H. Natter, S. Diebels, E. Lach, R. Hempelmann, Adv. Eng. Mater. 13 (2010) 23–28.
[15] W. Wang, R. Burgueño, J.-W. Hong, I. Lee, Mater. Sci. Eng. A 572 (2013) 75–82.
[16] E.O. Hall, Proc. Phys. Soc. Sect. B 64 (1951) 747–753.
[17] N.J. Petch, J. Iron Steel Inst. 174 (1953) 25–28.
[18] M. Klein, A. Hadrboletz, B. Weiss, G. Khatibi, Mater. Sci. Eng. A 319 (2001) 924–928.
[19] S. Zhang, M. Sakane, T. Nagasawa, K. Kobayashi, Procedia Eng. 10 (2011) 1497–1502.
[20] Y.W. Cheng, D.T. Read, J.D. McColskey, J.E. Wright, Thin Solid Films 484 (2005) 426–432.
[21] D.S. Gianola, S. Van Petegem, M. Legros, S. Brandstetter, H. Van Swygenhoven, K.J. Hemker, Acta Mater. 54 (2006) 2253–2263.
[22] A. Jung, H. Natter, R. Hempelmann, E. Lach, US Patent Application 13/377,021, United States, 2010.
[23] W. Chen, F. Lu, D.J. Frew, M.J. Forrestal, J. Appl. Mech. 69 (2002) 214–223.
[24] U.S. Lindholm, J. Mech. Phys. Solids 12 (1964) 317–335.
[25] J.F. Shackelford, Introduction to Materials Science for Engineers, Prentice Hall, Upper Saddle River, NJ, USA, 2008.
[26] M.T. Perez-Prado, J.J. Vlassak, Scr. Mater. 47 (2002) 817–823.
[27] Y. Xiang, T.Y. Tsui, J.J. Vlassak, J. Mater. Res. 21 (2006) 1607–1618.
[28] H.E. Swanson, Standard X-Ray Diffraction Powder Patterns, US Department of Commerce, National Bureau of Standards, Washington, DC, 1953.
[29] P. Scherrer, Gessell. Wiss. Gottingen Nachr. Math-Phys. Klasse 26 (1918) 98–100.
[30] Abaqus Documentation 6.11, Dassault Systemes Simulia Corp, 2011.
[31] J. Zhou, S. Allameh, W.O. Soboyejo, J. Mater. Sci. 40 (2005) 429–439.